ELSEVIER

Surface Science 418 (1998) 219–239

surface science

Electron affinity and work function of differently oriented and doped diamond surfaces determined by photoelectron spectroscopy

L. Diederich *, O.M. Küttel, P. Aebi, L. Schlapbach

University of Fribourg, Physics Department, Pérolles, 1700 Fribourg, Switzerland

Received 6 April 1998; accepted for publication 2 September 1998

Abstract

We investigate band bending, electron affinity and work function of differently terminated, doped and oriented diamond surfaces by X-ray and ultraviolet photoelectron spectroscopy (XPS and UPS). The diamond surfaces were polished by a hydrogen plasma treatment and present a mean roughness below 10 Å. The hydrogen-terminated diamond surfaces have negative electron affinity (NEA), whereas the hydrogen-free surfaces present positive electron affinity (PEA). The NEA peak is only observed for the boron-doped diamond (100)-(2 × 1):H surface, whereas it is not visible for the nitrogen-doped diamond (100)-(2 × 1):H surface due to strong upward band bending. For the boron-doped diamond (111)-(1 × 1):H surface, the NEA peak is also absent due to the conservation of the parallel wavevector component ($k_{\parallel}$) in photoemission. Electron emission from energy levels below the conduction band minimum (CBM) up to the vacuum level E_{vac} allowed the electron affinity to be measured quantitatively for PEA as well as for NEA. The emission from populated surface states forms a shoulder or a peak at lower kinetic energies, depending on the NEA behavior and additionally shows a dispersion behavior. The low boron-doped diamond (100)-(2 × 1):H surface presents a high-intensity NEA peak with a FWHM of 250 meV. Its cut-off is situated at a kinetic energy of 4.9 eV, whereas the upper limit of the vacuum level is situated at 3.9 eV, resulting in a NEA of at least −1.0 eV and a maximum work function of 3.9 eV. The high-boron-doped diamond (100) surface behaves similarly, showing that the NEA peak is present due to the downward band bending independent of the boron concentration. The nitrogen-doped (100)-(2 × 1):H surface shows a low NEA of −0.2 eV but no NEA peak due to the strong upward band bending. The (111)-(1 × 1):H surface does not show a NEA peak due to the $k_{\parallel}$ conservation in photoemission; E_{vac} is situated at 4.2 eV or below, resulting in a NEA of at least −0.9 eV and a maximum work function of 4.2 eV. The high-intensity NEA peak of boron-doped diamond seems to be due to the downward band bending together with the reduced work function because of hydrogen termination. Upon hydrogen desorption at higher annealing temperatures, the work function increases, and NEA disappears. For the nitrogen-doped diamond (100) surface, the work function behaves similarly, but the observation of a NEA peak is absent because of the surface barrier formed by the high upward band bending.

Keywords: Diamond; Hydrogen; Low-energy electron diffraction; Low-index single crystal surfaces; Photoelectron spectroscopy; Surface structure

* Corresponding author. Present address: University of Milan, INFM-Department of Physics, via Celoria 16, I-20133 Milan, Italy. Fax: +39 02 239 24 87; e-mail: diederich@mi.infn.it

0039-6028/98/$ – see front matter
PII: S0039-6028(98)00718-3

1. Introduction

1.1. Interest

Important progress in chemical vapor deposition (CVD) [1–4] of diamond in order to produce (100) and (111) oriented, textured, and p-type films together with the negative electron affinity (NEA) characteristics of these surfaces, has created a great deal of interest in developing NEA diamond-based electronic devices for high-speed, high-temperature and high-power applications such as electron multipliers, flat panel displays, cold cathodes, field emitters and photoemitters.

Doping diamond with electrically active impurities (n- and p-type) is necessary for many of these semiconductor device applications. The boron-doped (rare in nature, also produced synthetically; noted B-doped and called type IIb) diamond is the only single crystal with electronically active impurities. The B-doped, type IIb diamond shows p-type semiconductor properties with an acceptor level situated at 0.37 eV [1] above the valence band maximum (VBM). Until recently, no shallow n-type dopants have been found, although n-type behavior of diamond doped with nitrogen, phosphorus, sodium and lithium has been reported or predicted [3]. As a matter of fact, in most cases, the n-type behavior was associated with defects created during the introduction of the impurities (ion implantation). Accordingly, these semiconducting properties could not be sustained following high-temperature annealing. Very recently, however, Koizumi et al. [5] reported on n-type semiconducting diamond thin films with an activation energy of only 0.4 eV obtained by microwave plasma CVD using phosphine as a dopant source. Further research for n-type doping of diamond looks again more promising.

In type Ib diamond, the electron level due to substitutional nitrogen is situated 1.7 eV below the conduction band minimum (CBM) [6,7], i.e. it forms a deep donor level that is electronically inactive at room temperature as an n-type dopant but plays an important role in the recombination and compensation of electrical carriers. Very recently, Okano et al. [8] reported on heavily N-doped ($10^{20}\,cm^{-3}$) diamond films grown by CVD that show field emission of electrons at a threshold voltage less than $0.5\,V\,\mu m^{-1}$, which augurs well for cold-cathode technology.

The type Ib diamond received a lot of interest when Geis et al. [9] reported on field emission of electrons from N-doped diamond. Generally, emission from B-doped diamond requires vacuum electric fields of 20–50 $V\,\mu m^{-1}$ [9]. The measurements of Geis et al. [9] show that the N-doped diamond requires only fields of 0–1 $V\,\mu m^{-1}$. In order to explain this behavior, a NEA of 0.7 eV was assumed for this type of diamond and 1.7 eV for the O–Cs-treated diamond [10]. Recently, the same group presented a cold-cathode emitter based on a field-emission Spindt cathode, using a diamond film doped by substitutional nitrogen [11]. The device shows high field emission currents with little or no electric field 0–1 $V\,\mu m^{-1}$. Such a Geis–Spindt diamond field-emitter has also been studied theoretically [12]. The cathode performance is limited by the injection of electrons into diamond from the back-metal contact, whereas the emission performance is explained by the stable NEA of diamond, which allows the injected electrons in the diamond to be emitted into vacuum with electric fields of 0–1 $V\,\mu m^{-1}$.

1.2. Outline of the paper

In this paper, we present electron affinity χ and work function ϕ measurements of the differently doped and terminated diamond (100) and (111) surfaces by means of photoelectron spectroscopy. Section 3 describes the experimental methods, and Section 4 presents and discusses the band bending, the electron affinity and the work function measurements of the differently terminated, doped and oriented diamond surfaces. In Section 5, we draw our conclusions.

2. Electron affinity

Electrons in the conduction band are generally prevented from escaping into vacuum by the electron affinity barrier χ. However, some materials show a negative electron affinity (NEA) [13,14]. Bell [14] distinguished between true and effective

NEA. True NEA is defined if the vacuum level (E_{vac}) lies below the conduction band minimum (CBM) at the surface, and hence, electrons excited into the conduction band can easily escape into vacuum. The conventional semiconductors (Si, Ge, GaAs, GaP, InP,…) do not show true NEA [14]. However, adsorbing CsO, forming a surface dipole layer, which induces a short downward band-bending width (due to the heavy p-type doping) can reduce the affinity by several eV [14]. This results in a so-called effective NEA [14–17].

Himpsel et al. [18] first demonstrated in 1979 true NEA for the hydrogen-terminated (H-terminated) diamond (111) surface [(111)-(1×1):H surface] by a photoelectric threshold at the band-gap energy of 5.5 eV and by the sharp peak observed at low kinetic energies, characteristic for the emission of thermalized photoelectrons from the CBM. However, the hydrogen-free (H-free) (111) reconstructed surface [(111)-(2×1) surface] shows a positive electron affinity (PEA) [13,19].

In 1994, Van der Weide et al. [20] found that the diamond NEA effect is not only limited to the (111) surface but also present for the (100) surface. The monohydride (100) reconstructed surface [(100)-(2×1):H surface] also exhibits NEA, as reported earlier by other groups [20–22] and by our group [23], whereas the H-free (100) reconstructed surface [(100)-(2×1) surface] shows PEA. Adsorption of thin metallic layers (Ti [24], TiO [25,26], Ni [27], Cu [27] and Co [27] and Cs [28]) on the H-free PEA diamond (100) and (111) surfaces results in the reappearance of NEA. Qualitatively, these experimental results agree with the calculations made for diamond surfaces by Pickett [29] and Zhang et al. [30]. Using self-consistent local-density-based methods, Pickett [29] showed that caesiation of the PEA-oxygenated diamond (100) surface changes it to a nearly metallic surface with -0.85 eV true NEA and a ϕ of 1.25 eV. Zhang et al. [30] obtained, using ab-initio molecular-dynamics calculations, a PEA of 0.8 eV for the (100)-(2×1) surface, whereas the (100)-(2×1):H surface presented a true NEA of -2.2 eV.

NEA effects are not only limited to diamond but are a general phenomenon of wide-band-gap semiconductors. Thin films of condensed hexatriacontane (paraffin wax) [31], LiF films on Ge(100) [32], AlN films on 6H–SiC [33] and c-BN powder and films [34] were shown to exhibit a NEA.

3. Experimental

3.1. Electron spectroscopy for chemical analysis (ESCA) apparatus

The hydrogen-plasma-cleaned crystals are mounted on a heatable (up to 1200°C) sample holder and transferred to a VG ESCALAB Mk II spectrometer with a base pressure of 2×10^{-11} mbar, equipped with a MgKα ($h\nu=1253.6$ eV) and SiKα ($h\nu=1740.0$ eV) twin anode, a helium discharge lamp (He I, $h\nu=21.2$ eV; He II, $h\nu=40.8$ eV) and a LEED system. The energy resolution is at its best 0.9 eV for X-ray photoelectron spectroscopy (XPS) and 35 meV for ultraviolet photoelectron spectroscopy (UPS, He I). A motorized goniometric sample manipulator allows polar and azimuthal rotations to be performed [35]. Photoelectron diffractogramms obtained from the diamond (100) and (111) surfaces allow a precise orientation of the crystal [36].

Annealing temperatures of the diamond sample were measured with a two-color pyrometer, which was previously calibrated with a thermocouple. We annealed the diamond surfaces to temperatures up to 1100°C at pressures remaining in the 10^{-10}-mbar range, whereas the XPS and UPS (only for the boron-doped diamonds) measurements were performed at room temperature. Since the nitrogen-doped diamond (100) surface is insulating at room temperature, the charging effects were compensated for by illuminating the crystal by an argon ion laser ($\lambda=514$ nm, $P=25$ mW) for the XPS measurements and by performing the UPS measurements at a substrate temperature of 400°C [37]. The measurements at 400°C were performed in a mode with alternating heating and measuring cycles (50 Hz) to avoid disturbing the electric and magnetic fields due to the sample heating current.

3.2. Sample description and preparation

The diamond substrates used in this study are a nitrogen-doped, type Ib (noted N-doped, $N_D = 10^{20}\,cm^{-3}$) 3×4 mm synthetic (100) and boron-doped, type IIb (noted B-doped, $N_A = 10^{16}$ and $10^{20}\,cm^{-3}$) 5×5 mm natural (100) and (111) crystals. They are oriented within 3° of the (100) and (111) crystallographic planes, and the surface roughness of the as-received crystals is more than 2 nm RMS as shown by atomic force microscope (AFM) images (Fig. 1). {The definition of RMS roughness (standard deviation) is: RMS = $[\sum (z_i - z_{av})2/N]1/2$, where z_{av} = average of z_i, and N = number of points}. The surface-sensitive techniques to analyze the crystallographic and electronic structure require a very low surface roughness and no surface contamination. Our natural diamond surfaces were mechanically polished by Meyer AG (Anton Meyer & Co. Ltd., Biel, Switzerland) and afterwards cleaned by a microwave hydrogen plasma at 870°C and at a pressure of 40 mbar in order to smooth and to clean the surface [38]. After the microwave hydrogen plasma, the surface roughness of the crystals is less than 10 Å RMS (Fig. 1).

Neither of the surfaces shows surface contamination (less than 0.5 at.% of oxygen, which is the detection limit of the technique), as shown by the MgKα XP normal emission overview spectrum [23,37,39], even after several weeks in air. This means that they are stable in air [38,40]. The (100) surface presents a (2×1) reconstruction, as shown by the LEED patterns [21,38,40] and by the atomic resolution STM images [41] (Fig. 2, note that the two (2×1) domains rotated by 90° with respect to each other are clearly visible). The (111) surface shows a (1×1) reconstruction as shown by very-high-quality LEED patterns [19,38,39,42] and by the atomic resolution STM images as shown in Fig. 2 [43]. Our STM images show large, atomically flat terraces for the hydrogen plasma treated surfaces, which is an indication of the efficient surface polishing. Recently, Hayashi et al. [44] experimentally observed step-flow etching of diamond (100) surfaces by AFM and confirmed the polishing of diamond surfaces by hydrogen plasma treatment. The corrugated structure observed before the treatment disappears and atomic steps (several atoms high), running over the surface parallel to the [110] direction, appear. Therefore lateral propagation of multi-atomic steps takes place during hydrogen plasma etching.

The reference substrate is a copper (110) single crystal already polished and oriented within 0.5° of the (110) crystallographic plane. The cleaning process for the copper (110) surface consisted of repeated cycles of argon-ion bombardment at several decreasing energies between 1.5 and 0.5 keV, followed by annealing up to 600°C [45].

4. Results and discussion

4.1. Principle of UPS measurements for low-kinetic-energy electrons

In order to understand better the determination of electron affinity χ and work function ϕ in our UP spectra, we show in Fig. 3 combined He I and He II spectra and the corresponding energy band schemes for the NEA [Fig. 3a, for the diamond (100)-(2×1):H surface] and PEA [Fig. 3b, for the silicon (100) surface] cases, respectively. The emission width, w, from the low-kinetic-energy cut-off to the VBM can be used to calculate the electron affinity χ by:

$$\chi = h\nu - E_g - w$$

with $h\nu$ the photon energy and E_g the band gap. If a diamond surface shows NEA, then χ is negative and hence electrons thermalizing to the CBM are emitted very easily into the vacuum. They appear in the He I spectra as a sharp, high-intensity peak at low kinetic energies, and the energy position determines the CBM (because E_{vac} lies below it). The relative position of the CBM with respect to E_F is chosen by the position of the NEA peak with extrapolation to zero intensity within an error of 0.1 eV. This error value is estimated from the error for the determination of the energy position and by the reproduction of the results (surface preparation). Cardona and Ley [46] state that the energy at which the spectra extrapolates linearly to zero determines ϕ, and therefore they established this way of determining

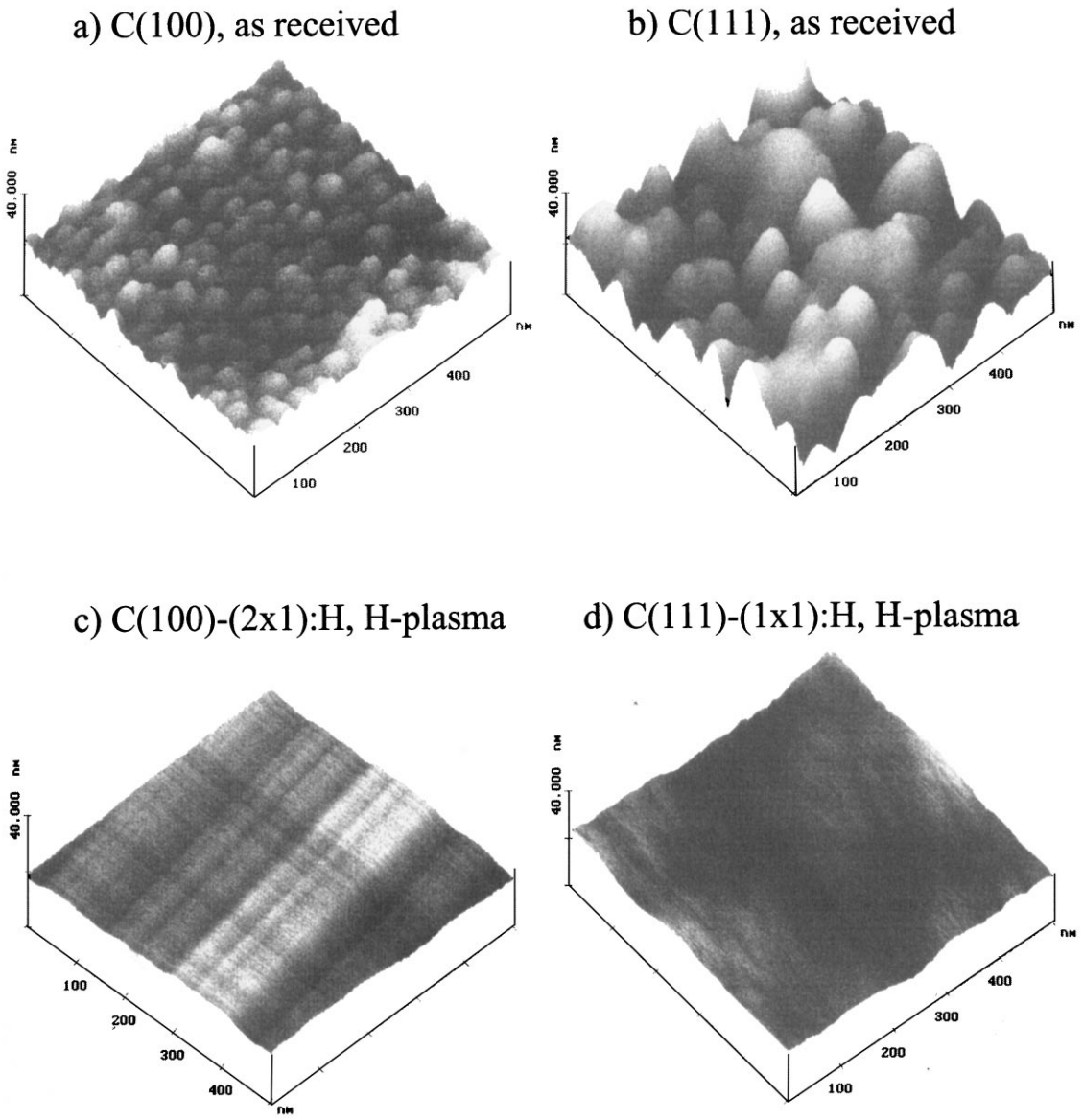

Fig. 1. Atomic force microscope tapping mode images of the diamond (100) and (111) surfaces. (a), (b) show the as-received (100) and (111) surfaces and (c), (d) the hydrogen-plasma treated diamond (100) and (111) surfaces, respectively.

energy levels for photoemission studies in semiconductors. From the diamond band gap of 5.5 eV, we can subtract the 4.9 eV of the NEA peak (the NEA peak characterizes the distance $E_F - CBM$), and the resulting 0.6 eV characterizes the energy distance at the surface between the VBM and E_F. The origin of the low-kinetic-energy peak at approximately 3.9 eV will be discussed in Section 4.3.4.

However, depending on the spectrometer used, these low-kinetic-energy electrons cannot overcome the work function of the electron analyzer and, hence, cannot be detected. Therefore, a small negative bias voltage between -0.5 and -5.0 V

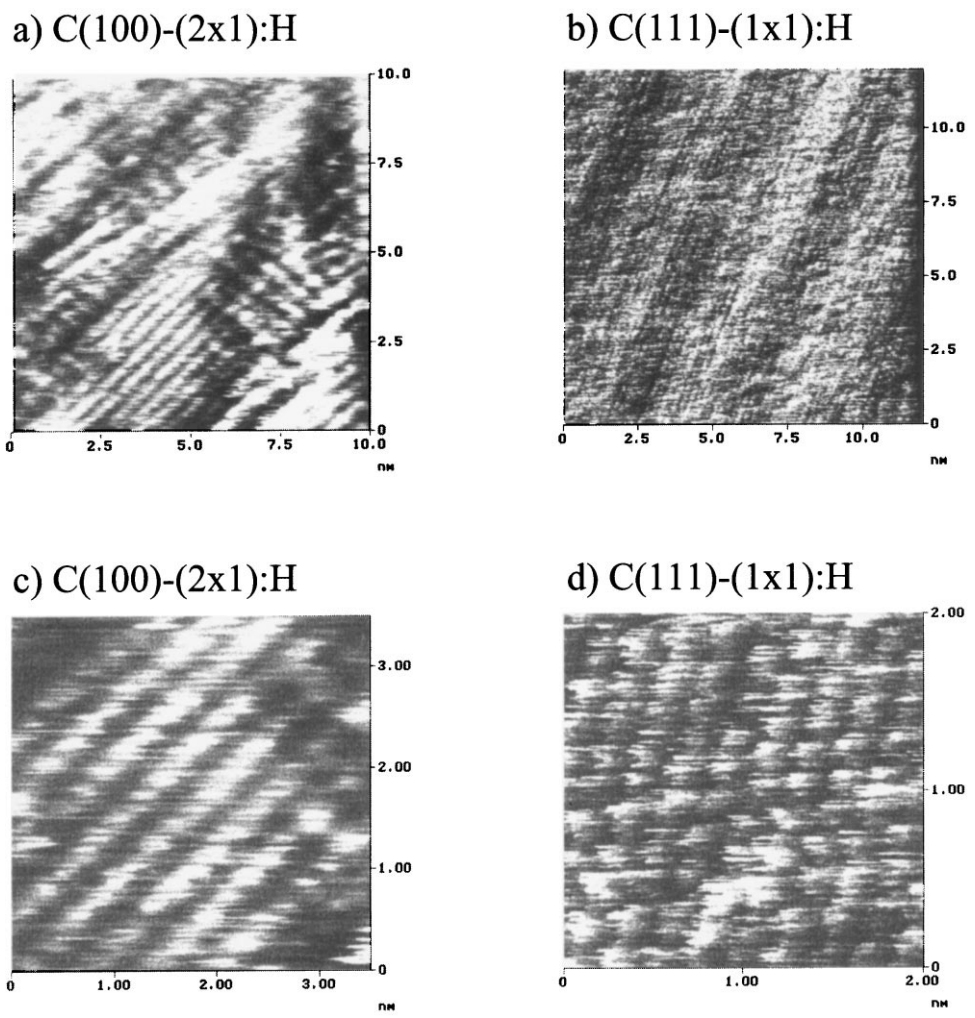

Fig. 2. Scanning tunneling microscope current images of the hydrogen-plasma treated diamond (100) and (111) surfaces. Whereas, in (a), the two domains of the (2×1) reconstructed (100) surface are visible, in (c), the dimer rows with a separation of 5 Å are visible. In (b) and (d), the (1×1) reconstruction of the (111) surface is visible covering the threefold symmetry.

is applied to the sample [23,37,39,47]. This applied bias voltage also eliminates the problem of secondary emission from the walls of the sample chamber and other parts of the spectrometer [46]. For PEA, E_{vac} is above the CBM and, therefore, the low-kinetic-energy cut-off in the spectra determines E_{vac}. Both, the NEA (for the diamond (100)-(2×1):H surface) and PEA (for the copper (110) surface) cases are illustrated by the He I spectra in function of the applied bias (Fig. 4). For an applied bias of -1.5 V or below, the cut-off positions of the spectra do not change any further. The intensity only increases in function of the applied bias voltage due to the increased electric field between sample and analyzer. The spectra change (induced by the higher ϕ_A of the electron analyzer) due to the applied bias is shown in Fig. 5 for three different applied bias voltages. Below -1.5 V, we can measure the whole spectra up to E_{vac}.

For diamond surfaces, the states near E_F are better illustrated by the He II spectra [47]. The

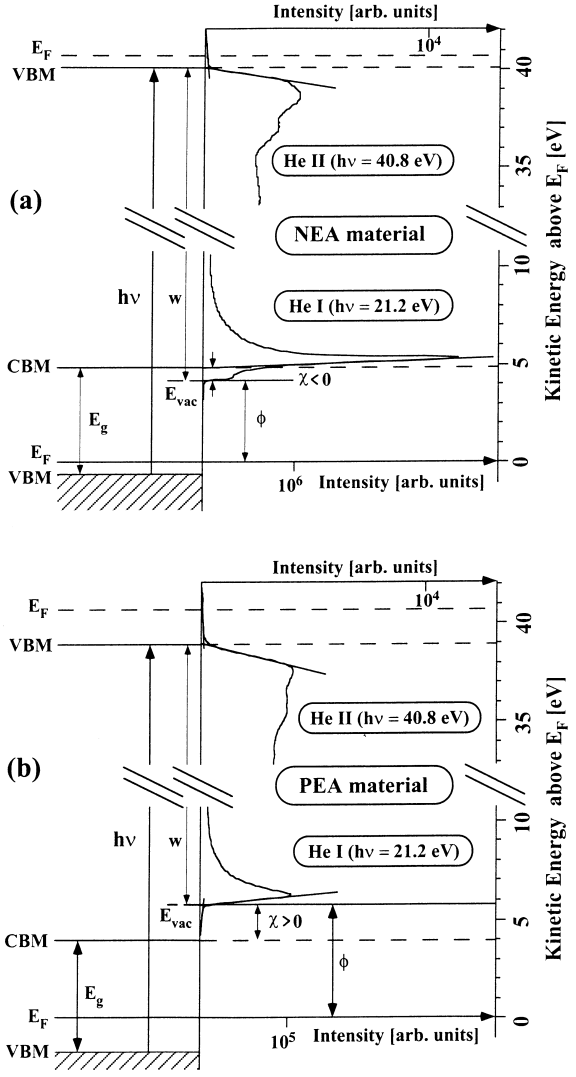

Fig. 3. Combined He I ($h\nu = 21.2$ eV) and He II ($h\nu = 40.8$ eV) normal emission spectra of the valence band for (a) negative electron affinity (NEA) and (b) positive electron affinity (PEA) materials with the band diagrams on the left side, respectively. We determine the spectra cut-off with extrapolation to zero intensity. Labeled are the work function, ϕ, the electron affinity, χ, the band gap, E_g, the vacuum level, E_{vac}, the photon energy, $h\nu$, the Fermi level E_F, the conduction band minimum (CBM) and the valence band maximum (VBM). Note the different intensity scales for the (a) NEA and (b) PEA cases.

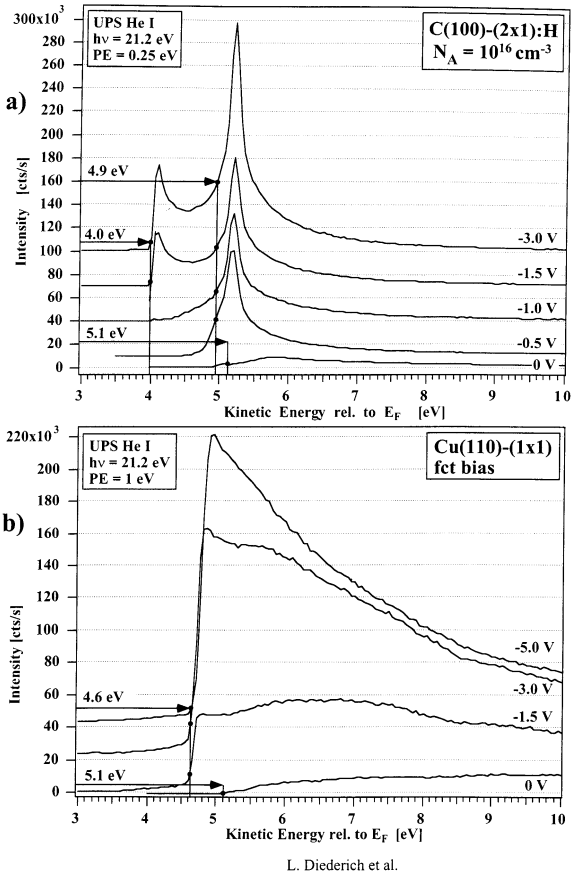

Fig. 4. Low kinetic-energy part of the He I ($h\nu = 21.2$ eV) normal emission spectra showing the valence band of the (a) low boron-doped diamond (100)-(2 × 1):H surface and the (b) copper (110)-(1 × 1) surface for different applied biases voltages to overcome the work function of the analyzer. The numbers given in the graph represent the cut-off energy position of the NEA peak and of the spectra, respectively.

reason for this is the more favorable photoemission cross-sections for He II. The cross-section of the 2p states at 8.0 eV binding energy is lower for the photon energy of 40.8 eV compared to 21.2 eV, but it is higher for states near E_F. If surface states are not present, then we can determine the VBM position near E_F in the He II parts of the spectra discussed elsewhere [13,37].

4.2. Principle of XPS measurements for the characterization of band bending

The knowledge of the bulk Fermi-level position is an important issue for a better understanding of the band bending and the energy band diagrams.

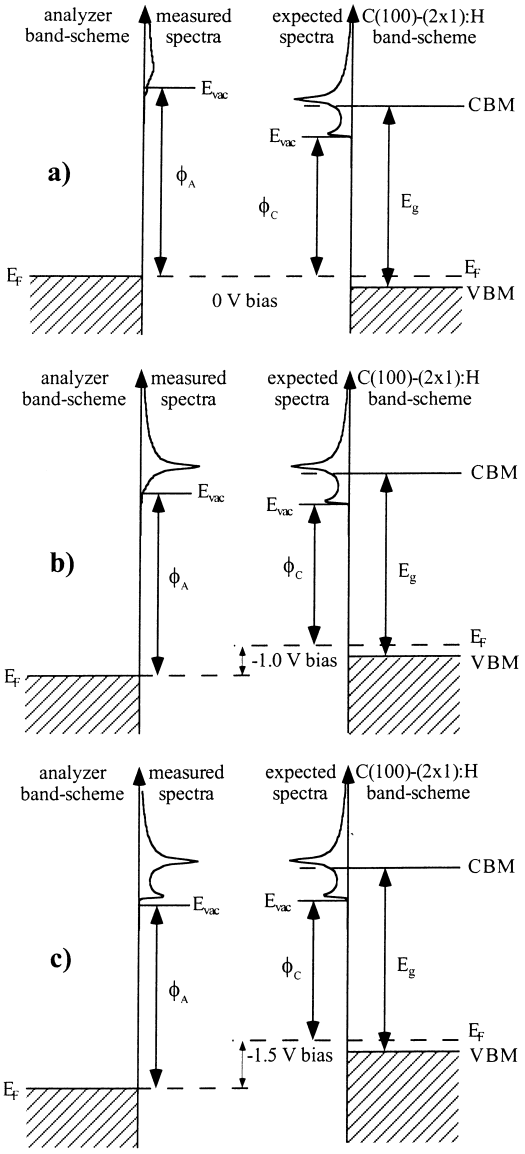

Fig. 5. Emission model showing on the right side the He I ($h\nu = 21.2$ eV) normal emission spectrum of the valence band for the diamond (100)-(2 × 1):H surface with the corresponding energy band diagram, and on the left side, the evolution of the measured spectra with increasing applied voltage [from 0 to −1.5 V corresponding to (a)– (c)].

It is known that boron forms the acceptor level in the type IIb diamond with an ionization energy of $E_A = 0.37$ eV [1,48,49]. By requiring charge neutrality, Bandis and Pate [13,50] calculated the bulk Fermi-level position of B-doped diamond as a function of temperature and impurity concentration. For the B-doped diamond, our analogous calculations predict the bulk Fermi level at 0.3 eV ($N_A = 10^{16}$ cm^{-3}) and at 0.25 eV ($N_A = 10^{20}$ cm^{-3}) [51] above the VBM in agreement with the calculations of Bandis and Pate [13,50]. The nitrogen forms a deep donor level in the type Ib diamond with an ionization energy of $E_D = 1.7$ eV [6]. For the N-doped ($N_D = 10^{20}$ cm^{-3}) diamond, our calculations predict the bulk Fermi level at 1.6 eV [51] below the CBM, 0.1 eV above the deep donor level (situated 1.7 eV below the CBM).

Another important component is the width of the band-bending region. Bandis and Pate [13,50] calculated this band-bending width, D, using the following formula [52]:

$$D = \sqrt{2\epsilon\psi/qN_A}$$

with ϵ the dielectric constant, ψ the band bending in eV and N_A the acceptor concentration. In Table 1, we present for diamond surfaces calculated band-bending widths for typical band bending and doping concentration. With a detection depth around 30 Å for the XPS analysis, we measure the whole band-bending region for a band bending of 1 eV and a doping concentration of 10^{20} cm^{-3}.

Changes in band bending, with different annealing temperatures successively removing hydrogen from the diamond surfaces, are illustrated by the XP normal emission spectra of the C 1s core level in Ref. [23] for the low-B-doped ($N_A = 10^{16}$ cm^{-3}) diamond (100) surface, in Ref. [53] for the low-B-doped ($N_A = 10^{16}$ cm^{-3}) diamond (111) surface, in

Table 1
Calculated band-bending widths for different band bending and different doping concentrations with the dielectric constant $\epsilon = \epsilon_r \cdot \epsilon_0 = 5 \times 10^{-11}$ and the charge $q = 1.6 \times 10^{-19}$ C

	$N = 10^{16}$ cm^{-3}				
ψ (eV)	0.1	0.3	0.5	1.0	1.2
D (Å)	800	1400	1800	2500	2750
	$N = 10^{20}$ cm^{-3}				
ψ (eV)	0.3	1.0	1.3	1.7	2.6
D (Å)	14	25	29	33	40

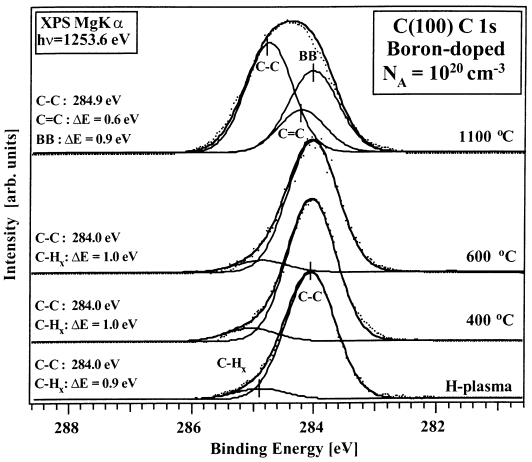

Fig. 6. XP normal emission spectra (MgKα, $h\nu = 1253.6$ eV) of the C 1s core level obtained after heating the high boron-doped diamond with hydrogen-terminated (100) surface to temperatures up to 1100°C.

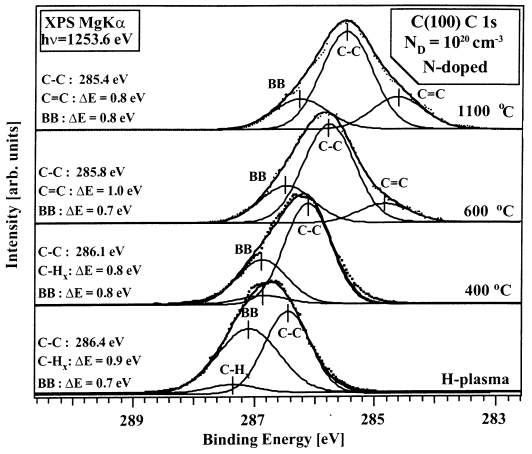

Fig. 7. XP normal emission spectra (MgKα, $h\nu = 1253.6$ eV) of the C 1s core level obtained after heating the high nitrogen-doped diamond with hydrogen-terminated (100) surface to temperatures up to 1100°C.

Fig. 6 for the high-B-doped ($N_A = 10^{20}\,cm^{-3}$) diamond (100) surface and finally in Fig. 7 for the high-N-doped ($N_D = 10^{20}\,cm^{-3}$) diamond (100) surface. The XPS measurements have been performed at room temperature for the B-doped crystals and at 400°C for the N-doped crystal. The Gaussian fits of the C 1s core levels using a full width of half maximum (FWHM) of 1 eV (bulk and surface contributions) were done to determine the position of the C–C, C=C and C–H_x ($1 \le x \le 3$) contributions.

The C–C contribution for the low-B-doped (100)-(2 × 1):H surface is situated at a binding energy of 284.0 eV and shifts successively towards higher binding energies [284.9 eV for the (100)-(2 × 1) surface]. For the (100)-(2 × 1) surface, the π-bonded dimers are responsible for the formation of surface states [19,47] and visible by the C=C contribution. The C 1s core levels for the low-B-doped (100) and (111) surfaces have nearly the same shape and position.

The shape and position of the C 1s core level of the differently B-doped (100) surfaces are nearly the same. However, for the H-free surfaces, the C 1s core level shape of the high-B-doped surface is larger as shown in Fig. 6. The hydrogen desorbing process remains the same, but the band-bending width is in the region of 30 Å, characteristic of the detection depth of the XPS analysis. This short band-bending width is due to the high doping concentration of boron ($N_A = 10^{20}\,cm^{-3}$) and the large band bending of 1.2 eV (Table 1). Due to this short band-bending width, we probe C–C bonds with slightly different binding energies. Hence, for the high-B-doped (100)-(2 × 1) surface (Fig. 6) with a band bending of 1.2 eV, a photoelectron from 20 Å below the surface shows a different binding energy to that of a photoelectron from the topmost surface. The additional C–C contribution due to the probed band bending is noted BB and situated at lower binding energies (because of the downward band bending). For the (100)-(2 × 1):H surfaces, the measured C 1s core levels are nearly the same because the energy bands show only a weak band bending of 0.3 eV.

In Fig. 7, the C–C contribution for the N-doped (100)-(2 × 1):H surface is situated at a binding energy of 286.4 eV and shifts successively towards lower binding energies [285.4 eV for the (100)-(2 × 1) bare surface]. As for the B-doped (100)-(2 × 1) surface, the π-bonded dimers are responsible for the formation of surface states [19,47] and visible by the C=C contribution. Nitrogen acts as a donor and, therefore, the electrons of the high-lying bulk donor levels populate the lower-lying unoccupied surface states. Due to this charge

transfer, E_F drops (therefore upward band bending), and the surface bands fill until thermodynamic equilibrium is achieved. Because the density of surface states N_D ($\sim 10^{15}$ cm^{-2}) is large, E_F of the (100)-(2×1) surface is pinned independently of the bulk dopant density. The shifts of the bulk C 1s core levels for the differently terminated N-doped (100) surfaces lead to an increasing upward band bending and therefore to a change in surface Fermi-level pinning. Similar to the high-B-doped (100)-(2×1) surface, the C 1s core level of the N-doped (100)-(2×1):H surface is larger, even with the same C–H_x contribution as for the B-doped surfaces [23,53]. Due to the high doping concentration of nitrogen ($N_D = 10^{20}$ cm^{-3}) and the large band bending, the whole band-bending width is probed, showing C–C bonds with slightly different binding energies. Therefore, an additional contribution at higher binding energies due to the large upward band bending (noted BB) has to be fitted. The (100)-(2×1) surface shows two shoulders, one at lower binding energies due to the H-free π-bonded dimer chains (as for the B-doped surface) [19,54,55]. At higher binding energies, the other shoulder is because of the large band bending probed by XPS due to the short band-bending width.

Now, it is interesting to simulate the C–C surface and C–C bulk (noted BB in the Figs. 6 and 7) contributions of the high-B- and N-doped diamond surfaces. These C–C contributions with slightly different binding energies are due to the large band bending which is probed because of the small band-bending width. We simulated the band bending value for the asymmetric peak of the 400°C annealed high-N-doped diamond (100) surface. For the simulation, we assume a detection depth around 30 Å where the intensity is decreasing exponentially with the detection depth. In addition, a FWHM of 1 eV for each simulated peak is assumed, corresponding to the emission coming from a certain layer from the surface to the bulk. With an initial band bending, ψ_0, we have calculated the energy shifts of the simulated peaks for different layers from the surface to the bulk. For an optimal band bending value, ψ_0, the addition of these layer peaks results in a total simulated peak similar to the C 1s core level peak measured by XPS. For the 400°C annealed, high-N-doped, (100) surface, we obtain a good agreement between the measured and the simulated peak for an assumed band bending of 1.65 eV within an error of 0.2 eV as shown in Fig. 8. This error value results from the fact that an increase or a decrease in FWHM around 0.1 eV results in a decrease or an increase in band bending of 0.2 eV, respectively. The simulated band-bending values confirm the values determined earlier by UPS and by the C 1s shift [37]. They are summarized for the high-B- and N-doped diamond (100) surfaces in Table 2.

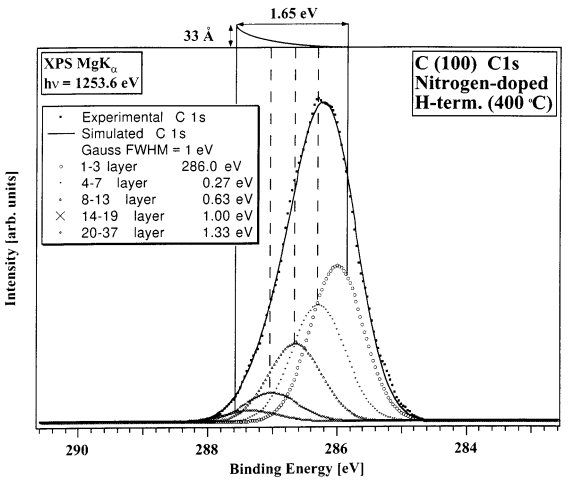

Fig. 8. Experimental and simulated C 1s core levels of the 400°C annealed, high nitrogen-doped diamond (100) surface. Agreement is achieved for a band bending value of 1.65 eV. The peaks formed by markers are the sum of the peaks formed by every layer from the surface to the bulk (listed in the legend). The corresponding C 1s band is shown above the graph.

Another interesting parameter, which can be fitted by these simulations is the doping concentration. We take the simulated band-bending value, and we vary the doping concentration and therefore the band-bending width. By doing the same fits, we can estimate the doping concentration. For the highly N- and B-doped crystals, agreement between the simulated and experimental peaks was achieved for a doping concentration of 10^{20} cm^{-3} with an error value of 0.3×10^{20} cm^{-3}.

Table 2
Simulated band bending (sBB) and band bending (BB) determined from the core level shifts of Refs. [23,53] and Figs. 6 and 7 and from the low kinetic-energy part of the He I normal emission spectra in Figs. 10–13 of the differently doped and oriented diamond surfaces

(a) Low-B-doped (100) surface				
T (°C)	H-plasma	400	600	1100
BB (eV)	0.3	0.5	0.6	1.2
(b) Low-B-doped (111) surface				
T (°C)	H-plasma	400	600	1100
BB (eV)	0.1	0.3	0.6	1.1
(c) High B-doped (100) surface				
T (°C)	H-plasma	400	600	1100
BB (eV)	0.3	0.3	0.3	1.2
sBB (eV)				1.35
(d) High N-doped(100) surface				
T (°C)	H-plasma	400	600	1100
BB (eV)	1.4	1.7	2.0	2.4
sBB (eV)		1.65	1.95	2.3

4.3. NEA of differently doped and oriented diamond surfaces

4.3.1. UPS characterization of the B-doped diamond (100) and (111) surfaces

Fig. 9 shows the low-kinetic-energy part of the He I normal emission spectra of the H-terminated and H-free low-B-doped diamond (100) and (111) surfaces. The spectra are aligned to the Fermi level and normalized to the bulk feature (situated around 13.0 eV kinetic energy), characterizing the p states [56–58]. The numbers given in the graph present the cut-off energy position with extrapolation to zero intensity [37]. At low kinetic energies, the monohydride terminated (100) and (111) surfaces show a high intensity with the spectra cut-offs at 3.9 and 4.2 eV, respectively. The cut-off energy position for the H-free surfaces is situated at higher kinetic energies around 5 eV. In contrast to the (111)-(1 × 1):H surface, the (100)-(2 × 1):H surface presents a sharp high-intensity peak (note the intensity scale of the graph) with a FWHM of 250 meV and with the cut-off situated at 4.9 eV

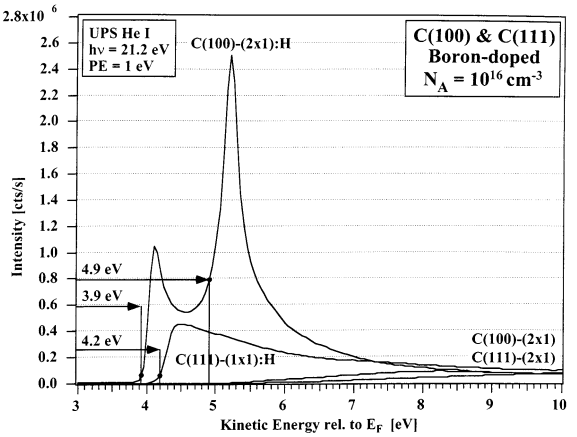

Fig. 9. Low kinetic-energy part of the He I ($h\nu = 21.2$ eV) normal emission spectra showing the valence band of the H-terminated and H-free low boron-doped diamond (100) and (111) surfaces. The energy scale is corrected for an applied bias voltage of −1.5 V to overcome the work function of the analyzer.

characterizing the NEA electrons coming from the CBM. The relative position of the CBM at the surface with respect to E_F is 4.9 eV. Subtracting $E_F - \mathrm{CBM} = 4.9$ eV from the band-gap (5.5 eV), we obtain 0.6 eV for the energy distance $\mathrm{VBM} - E_F$ and therefore a downward band bending of 0.3 eV [E_F of the low-B-doped diamond lies 0.3 eV above the VBM]. This downward band bending and the shifts determined from Ref. [23] allowed us to compute the band bending for the differently terminated low-B-doped (100) surface as listed in Table 2. For the other diamonds, we proceed in the same way, and the determined values are also listed in Table 2.

Figs. 10–12 show the low-kinetic-energy part of the He I normal emission spectra for the low-B-doped diamond (100) surface (Fig. 10), for the low-B-doped diamond (111) surface (Fig. 11) and for the high-B-doped (100) diamond surface (Fig. 12). After 400°C annealing of the low-B-doped (100)-(2 × 1):H surface (Fig. 10), the high-intensity peak has shifted to 4.7 eV, confirming the increasing downward band bending, whereas the intensity remains the same. The peak situated at 3.9 eV, characterizing the spectra cut-off, has decreased in intensity, whereas the position remains the same. After 600°C annealing, the cut-

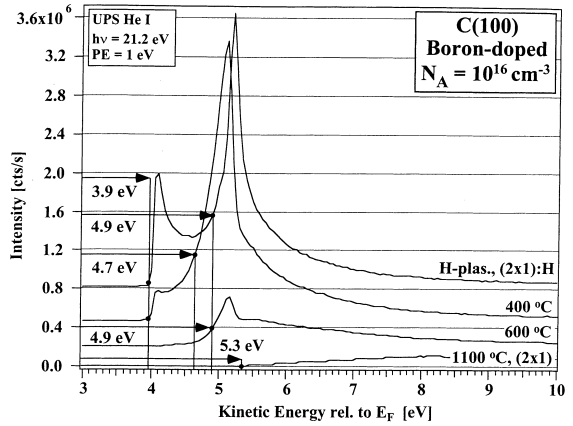

Fig. 10. Low kinetic-energy part of the He I ($h\nu = 21.2$ eV) normal emission spectra after heating the H-terminated low boron-doped diamond (100) surface to temperatures up to 1100°C. To overcome the work function of the analyzer, the energy scale is corrected for an applied bias voltage of -1.5 V.

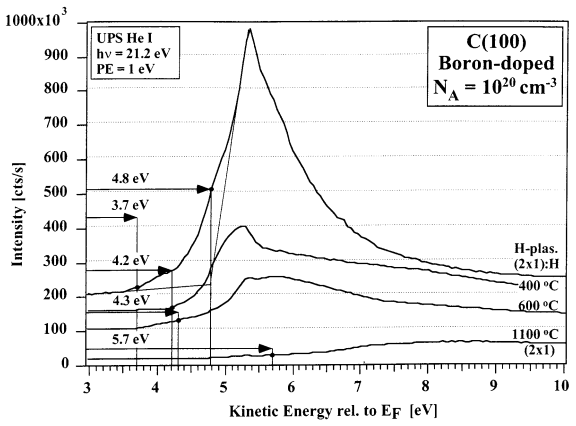

Fig. 12. Low kinetic-energy part of the He I ($h\nu = 21.2$ eV) normal emission spectra after heating the H-terminated high boron-doped diamond (100) surface to temperatures up to 1100°C. The energy scale is corrected for an applied bias voltage of -1.5 V to overcome the work function of the analyzer.

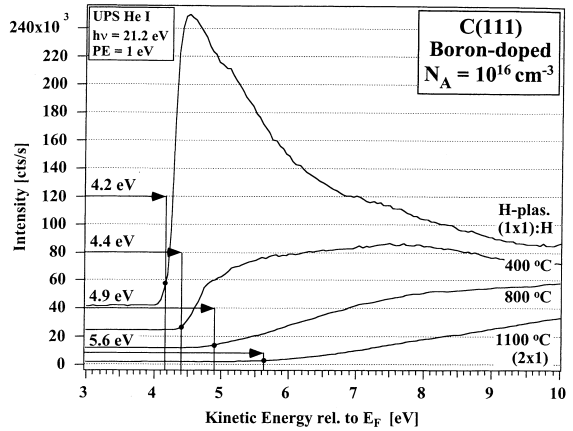

Fig. 11. Low kinetic-energy part of the He I ($h\nu = 21.2$ eV) normal emission spectra after heating the H-terminated low boron-doped diamond (111) surface to temperatures up to 1100°C. The energy scale is corrected for an applied bias voltage of -1.5 V to overcome the work function of the analyzer.

off position of the spectrum has shifted back to 4.9 eV similar to the NEA peak position, whereas the spectrum has decreased in intensity. The shifting reverses because the NEA peak successively vanishes after annealing up to 1100°C. A downward band bending of 0.6 eV (0.3 eV more than for the H-terminated surface, Table 2), equal to $\mathrm{VBM} - E_F = 4.6$ eV, means that E_{vac} lies in the band-bending region. Therefore, a PEA of 0.3 eV or a so-called effective NEA of -0.3 eV results. The (100)-(2×1) surface has its spectra cut-off situated at 5.3 eV, a band bending of 1.2 eV, and therefore results in a PEA of 1.3 eV as predicted by previous calculations [30].

The low-B-doped diamond (111)-(1×1):H surface shows a completely different behavior to that of the (100)-(2×1):H surface, as shown by the He I normal emission spectra in Fig. 11 and in Fig. 9 (note the intensities differences for both surfaces in Fig. 9). As shown in Fig. 9, the cut-off of the (111)-(1×1):H surface is situated at 4.2 eV, whereas the spectrum shows a weak shoulder at 5.0 eV, but we do not measure a high-intensity NEA peak around 4.9 eV as for the (100)-(2×1):H surface, even if E_F is nearly at the same position (Table 2). The cut-off positions, after annealing the (111)-(1×1):H surface to 400 and 800°C, shift to 4.4 and 4.9 eV, respectively. Finally, the (111)-(1×1) surface has the cut-off situated at 5.6 eV, which means that the hydrogen-free (111) surface shows PEA (the cut-off at 5.6 eV is larger than the band gap), in agreement with previous calculations [30].

In Fig. 12, the He I spectra show the NEA behavior of the high-B-doped diamond (100) surface. For the high-B-doped diamond (100)-(2×1):H surface, the electron affinity behavior is

similar to the low-B-doped diamond (100)-(2×1):H surface, but the shape and intensity of the spectra are different (note the different intensity scale). The NEA peak has an intensity three times lower and is broadened (FWHM = 1 eV) with the cut-off situated at 4.8 eV, whereas the spectra cut-off is situated at 3.7 eV. The difference to the low-B-doped diamond can be explained by the fact that for the high-B-doped diamond, we probe practically the whole band bending width (15 Å), resulting in a more broadened peak. Another reason may be a greater surface roughness. After 600°C annealing, the cut-off position has shifted back to 4.3 eV, while the peak has decreased in intensity. The (100)-(2×1) surface has its cut-off situated at 5.7 eV and shows a PEA.

4.3.2. UPS characterization for the N-doped diamond (100) surface

An interesting question is whether the high-N-doped (with E_F situated at 1.6 eV below the CBM) diamond (100)-(2×1):H surface shows NEA like the B-doped diamond (100)-(2×1):H surfaces. He I normal emission spectra for the N-doped diamond (100)-(2×1):H surface and for the same surface after annealing up to 1100°C are shown in Fig. 13. The spectra cut-off of the (100)-(2×1):H surface is situated at 3.1 eV, but the spectra do not show a high-intensity NEA peak (note the different intensity scale). In fact, subtracting the energy distance $E_F - CBM = 3.1$ eV from the band-gap (5.5 eV), we obtain a value of 2.4 eV for the energy distance $VBM - E_F$. This energy distance is larger than that determined with the He II spectra [37], and a NEA of at least -0.2 eV results. The reason for the non-presence of the NEA peak will be discussed in Section 4.3.3. The cut-off position, after annealing up to 600°C, shifts to 3.3 eV, but the spectrum remains similar in shape and intensity. Finally, the (100)-(2×1) surface has its cut-off at 4.7 eV, resulting in a PEA of 0.5 eV [37], and the spectrum has decreased in intensity.

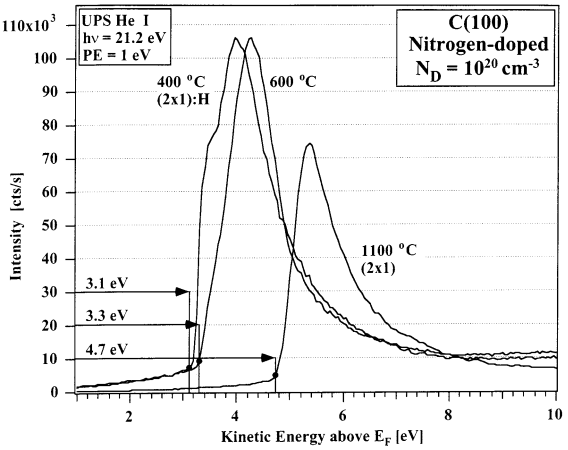

Fig. 13. Low kinetic-energy part of the He I ($h\nu = 21.2$ eV) normal emission spectra after heating the H-terminated high nitrogen-doped diamond (100) surface to temperatures up to 1100°C. The energy scale is corrected for an applied bias voltage of -1.5 V to overcome the work function of the analyzer.

4.3.3. Angle-resolved NEA measurements

Our UPS measurements reveal a high-intensity NEA peak for the low-B-doped diamond (100)-(2×1):H surface with a low-kinetic-energy cut-off at 3.9 eV, whereas the low-B-doped diamond (111)-(1×1):H and high-N-doped diamond (100)-(2×1):H surfaces do not reveal a NEA peak but have their cut-offs situated at 4.2 and 3.1 eV, respectively. In order to understand and interpret the photoemission data and to extract information about the electronic properties of the different diamond surfaces, we consider Spicer's three-step-process [59] for photoelectron emission from semiconductors consisting of (1) photoexcitation of the electrons by absorption of light, (2) transport of the electrons through the crystal to the surface, and (3) escape of the electrons from the surface into the vacuum. The escape mechanism is responsible for the photoelectron emission of CBM electrons and for the measurement of the NEA peak by means of UPS.

B-doped diamond is a semiconductor with an indirect band gap, which can affect the escape probability of electron emission for different oriented diamond surfaces. The CBM is at $k_{min} = 0.76k_x$ in the [100] direction [60] where k_x is the zone boundary wavevector. For the (100) surface, CBM electrons arrive with a zero component of the electron wave vector, which is parallel to the emission surface ($k_\parallel$). For the (111) surface, CBM electrons arrive with a large $k_\parallel$. Kane et al. [61,62] established an one-electron escape model

of electron emission from a perfect surface and require in this model not only the conservation of energy but also the conservation of $k_{\parallel}$. In addition, $k_{\parallel}$-conservation of NEA surfaces acts in some cases as a barrier for low-kinetic-energy electrons with a large $k_{\parallel}$. Bandis et al. [50,63] analyzed this constraint for the diamond (111) surface and found that χ must be less than -4.55 eV in order to satisfy the energy and $k_{\parallel}$ conservation. The emitted electrons with a large $k_{\parallel}$ component would imply a distinct threefold azimuthal angular distribution of emission, with little intensity directed along the surface normal. However, if χ is more than -4.55 eV, then the electrons are totally internally reflected at the diamond–vacuum interface. The fact that we do not measure a NEA peak for the low-B-doped (111)-(1×1):H surface suggests that χ is more than -4.55 eV. Therefore, due to the $k_{\parallel}$-conservation in photoemission, we expect at the CBM a higher electron-escape probability for the diamond (100) than for the (111) surface, which is in agreement with our UPS results (Fig. 9). We measured the angular distribution of the low-kinetic-energy electrons for the B-doped diamond (100)-(2×1):H and (111)-(1×1):H surfaces, as shown in Figs. 14 and 15, respectively. For the (100)-(2×1):H surface, the emitted electrons from the CBM (with an applied bias voltage of -1.5 eV), i.e. the angular distribution of the NEA peak, are directed along the surface normal with cylindrical symmetry and a FWHM of 35° (Fig. 14). The photoelectrons characterizing NEA behavior are emitted with a high intensity normal to the surface and with a sharp angular width. Increasing the applied bias voltage up to -10 V will focus these low-kinetic-energy electrons normal to the surface with a FWHM below 20°. For the (111)-(1×1):H surface with no measured NEA peak, the emitted electrons from the CBM show a ring with cylindrical symmetry and with a maximum at 22° polar angle. These measurements agree with the fact that we observe a higher electron-escape probability at the CBM for the diamond (100) than for the (111) surface at normal emission. The $k_{\parallel}$ constraint in photoemission and a NEA above -4.55 eV are the reasons why we do not detect a high-intensity NEA peak for the (111)-(1×1):H surface. The

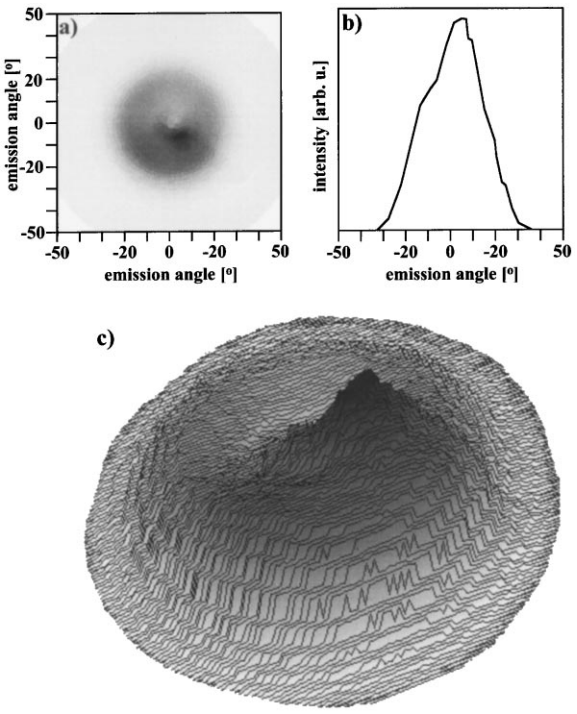

Fig. 14. Angular distribution [(a) intensity plot using a linear gray scale with maximum intensity in black and minimum intensity in white, (b) polar cut and (c) surface plot] of the low kinetic-energy emitted electrons ($h\nu=21.2$ eV) at 5.0 eV for the low boron-doped diamond (100)-(2×1):H surface. The distribution is directed along the surface normal with cylindrical symmetry and a FWHM of 35°.

different surface preparation and the high applied bias voltage by Bandis et al. [13] may be the reason why they did not measure the same angular distribution of CBM emitted electrons from the low-B-doped diamond (111)-(1×1):H surface.

Due to the $k_{\parallel}$-constraint in photoemission for the low-B-doped diamond (111) surface with little intensity directed along the surface normal, we show in Fig. 16 the low-kinetic-energy part of the He I normal emission spectra of the (111)-(1×1):H surface for different polar angles. From Figs. 15 and 16, we deduce 22° off normal as the intensity maximum (twice more than at normal emission). However, not only has the intensity increased, but also the spectrum cut-off has shifted to lower kinetic energies (3.9 eV), while it is situated at 4.2 eV for normal emission. The measured electrons emitted from the CBM suggest that the

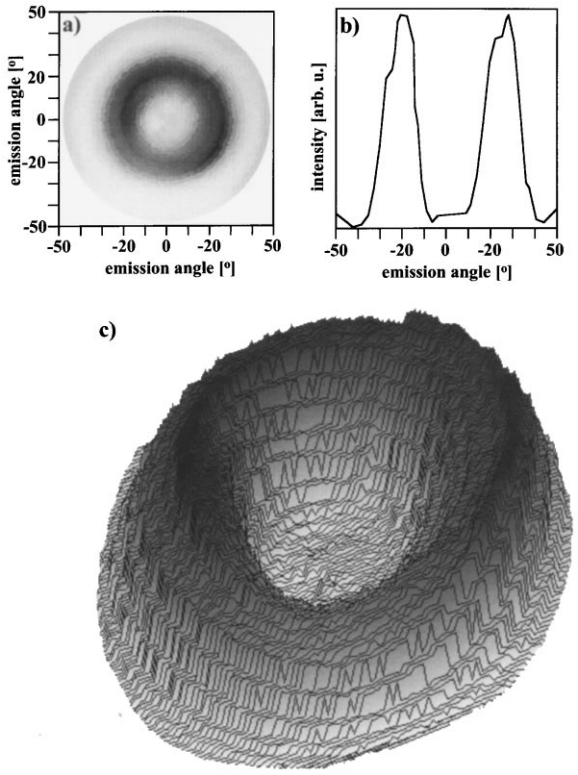

Fig. 15. Angular distribution [(a) intensity plot using a linear gray scale with maximum intensity in black and minimum intensity in white, (b) polar cut and (c) the surface plot] of the low kinetic-energy emitted electrons ($h\nu = 21.2$ eV) at 5.0 eV for the low boron-doped diamond (111)-(1 × 1):H surface. The distribution shows a ring with cylindrical symmetry and a maximum intensity at 22° polar angle.

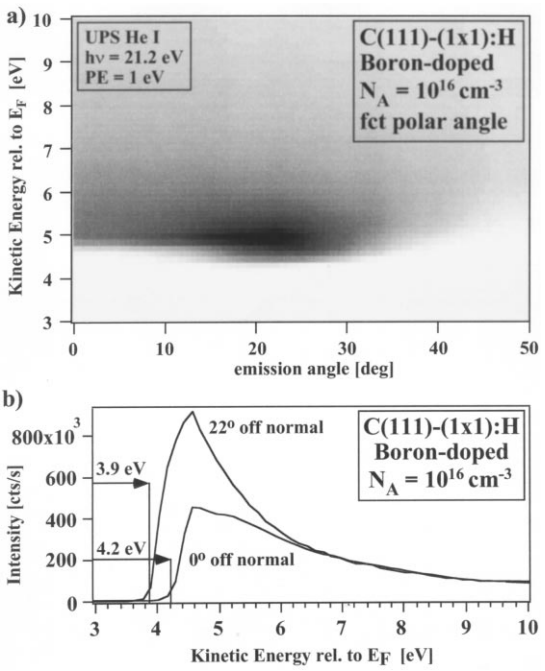

Fig. 16. (a) Intensity plot representing a series of energy spectra taken on a dense grid of polar angles using a linear gray scale with maximum intensity in black and minimum intensity in white, (b) low kinetic-energy part of the He I ($h\nu = 21.2$ eV) energy spectra taken at polar angles of 0 and 22°.

(111)-(1 × 1):H surface shows no NEA peak but NEA behavior. Similar to the diamond (111) surface, detection of the NEA silicon (111) surface using a special activation process was unsuccessful. Goldstein [17] did not succeed in measuring the activation of the silicon (111) surface to NEA using the same procedure (adsorption of Cs–O on the Si surface) as for the silicon (100) surface, but he did observe an increasing photoelectron emission efficiency due to the activation process.

For the N-doped diamond (100)-(2 × 1):H surface, the $k_{\parallel}$-conservation in the photoemission is not the mechanism preventing CBM electrons to be emitted into the vacuum. In this case, the upward band bending at the surface seems to be the responsible mechanism that produces an electric field responsible for preventing CBM electrons to escape into the vacuum. In fact, for the N-doped (100) surface, a strong upward band bending at the surface has been revealed (Table 2). A similar effect was observed by Spicer [59], who showed, using photoemission studies on alkali-antimony compounds, that the most efficient emitters are those with p-type behavior. Like the downward or upward band banding of B- or N-doped diamond, respectively, the bands of n-type alkali-antimony compounds have a tendency to turn upward at the surface reflected by an increase in the electron affinity barrier [59].

4.3.4. Emission from populated surface states

The low-kinetic-energy electron emission spectrum of the low-B-doped (100)-(2 × 1):H surface (Figs. 9 and 10) shows that below the NEA peak, there is a low-kinetic-energy peak or shoulder with its cut-off situated below the CBM. In

addition, the cut-off of the low-B-doped (111)-(1×1):H surface shows a dispersion with changing polar angle (Fig. 16). By secondary electron-emission spectroscopy, Yater et al. [64] also observed this low-kinetic-energy shoulder but for the caesiated diamond (100) surface. They suggested that for a strong NEA, low-kinetic-energy electrons at the surface that populate energy levels below the CBM can still be emitted into the vacuum [64]. The intensity and distribution of these low-kinetic-energy electrons depend on the specific mechanism of population. The inelastic scattering at the surface to the vacuum interface and the transitions of electrons from the CBM to unoccupied surface states, situated in the band gap, are potential possible mechanisms. Transitions of electrons from the CBM to unoccupied surface states situated in the band gap seem to be the most promising mechanism to explain the low-kinetic-energy shoulder for the B-doped diamond (100)-(2×1):H and (111)-(1×1):H surfaces with their cut-offs situated below the CBM. For the (100) surface, no experimental studies of the unoccupied surface states have yet been performed, whereas theoretical studies [65–67] show that the lowest unoccupied surface states are localized at the $\bar{\Gamma}$ point at 1 eV below the CBM. At normal emission, our spectra reveal a cut-off position at 3.9 eV (1 eV below the CBM), whereas at increasing polar angles, this cut-off position shifts to higher kinetic energies, showing an upward dispersion behavior in agreement with theoretical calculations [65]. For the (111) surface, very few studies of the unoccupied surface states have been performed [68,69]. Using soft X-ray absorption, Morar et al. [69] observed several absorption features in the bulk band gap below the 289.2-eV bulk-C 1s absorption edge associated with transitions from the C 1s surface core level to unoccupied surface states. Their modified energy-band dispersions, with a surface band gap of 2.1 eV at $\bar{J}$, present a minimum along $\bar{J}\bar{K}$. Our measurements (Fig. 16) show a dispersion of the low-energy cut-off with a minimum at a polar angle of 22°. Alternatively, by measuring these low-kinetic-energy electrons, we are always near the $\bar{\Gamma}$ point using the formula given in Ref. [47]. The dispersion of these low-kinetic-energy electrons for different polar angles is not well understood and needs further investigations.

Considering the low-kinetic-energy cut-off as the upper value of the vacuum level (it can even lie below) we can deduce, similar to Thomas et al. [23] and Yater et al. [64], an upper limit of the NEA value and a maximal work function for the different terminated, doped and oriented diamond surfaces, as shown in Table 3. For the low-B-doped diamond H-terminated (100) and (111) surfaces, the obtained NEA values (-1.0 eV and -0.9 eV) are slightly larger than those measured by Bandis and Pate [13,22] (-0.8 eV and -0.7 eV), whereas they partially agree with those measured by Thomas et al. [21] [-0.4 eV and 1.8 eV for the H-terminated and H-free (100) surfaces]. However, for the low-B-doped (100) surface, the electron affinity change of 2.3 eV, determined in Fig. 10, is similar to that observed by Thomas et al. (2.2 eV) [21], whereas it differs from the value calculated by Zhang et al. (3.0 eV) [30]. This may be due to an overestimated NEA value of -2.2 eV for the (100)-(2×1):H surface.

Table 3
Electron affinity (χ) and work function (ϕ) of the differently doped and oriented diamond surfaces determined in the low kinetic-energy part of the normal emission He I spectra from Figs. 10 and 13

(a) Low-B-doped(100) surface				
T (°C)	H-plasma	400	600	1100
χ (eV)	-1.0	-0.8	0.3	1.3
ϕ (eV)	3.9	3.9	4.9	5.3
(b) Low-B-doped(111) surface				
T (°C)	H-plasma	400	600	1100
χ (eVI	-0.9	-0.5	0.3	1.5
ϕ (eV)	4.2	4.4	4.9	5.6
(c) High B-doped(100) surface				
T (°C)	H-plasma	400	600	1100
χ (eV)	-1.1	-0.6	-0.5	1.8
ϕ (eV)	3.7	4.2	4.3	5.7
(d) High N-doped(100) surface				
T (°C)	H-plasma	400	600	1100
χ (eV)	/	-0.2	-0.3	0.7
ϕ (eV)	/	3.1	3.3	4.7

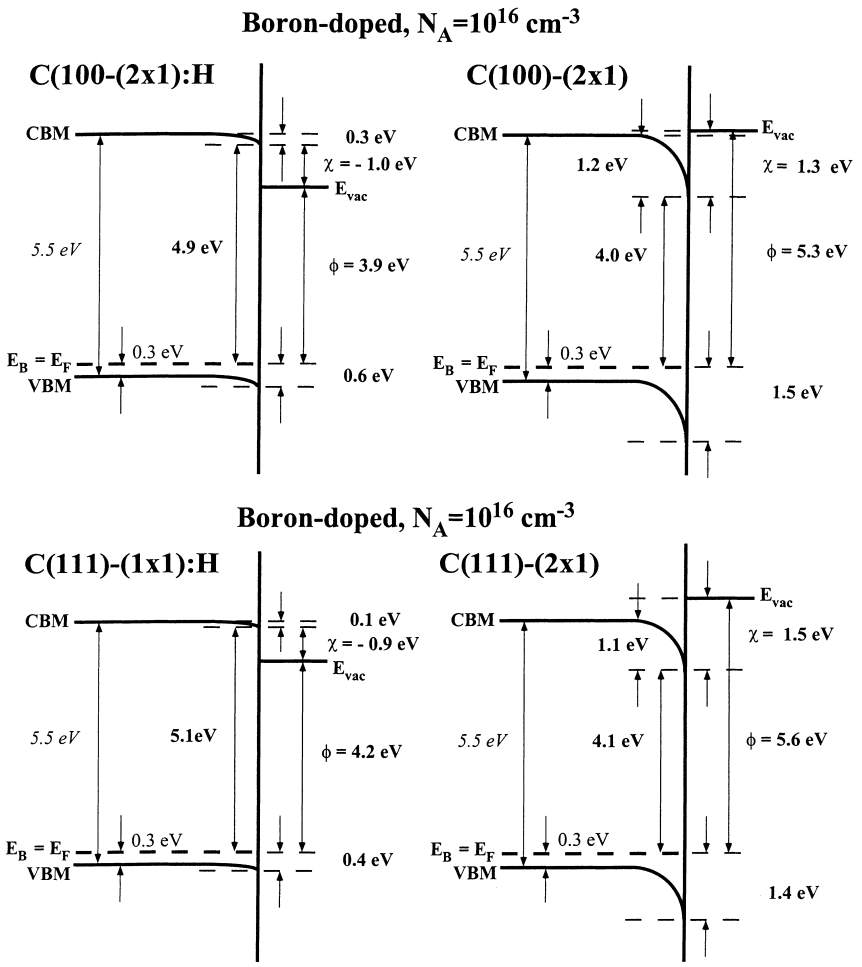

Fig. 17. Energy band diagrams of the low boron-doped H-terminated and H-free diamond (a) (100) and (b) (111) surfaces. The values are estimated to lie within an error value of 0.1 eV. The values from the literature are shown in italics, the calculated values in normal font and the measured values in bold.

4.3.5. Energy band diagrams

It is now interesting to summarize the values from the literature (band gap), the calculated values (bulk Fermi level and band bending width) and the measured values (band bending, electron affinity and work function) in the energy band diagrams for the differently terminated, doped and oriented diamond surfaces, as shown in Fig. 17 [low-B-doped diamond (100) and (111) surfaces] and in Fig. 18 [high-B- and N-doped diamond (100) surfaces]. For the B-doped diamond, our calculations predict the bulk Fermi level at 0.3 eV ($N_A=10^{16}\,cm^{-3}$) and 0.25 eV ($N_A=10^{20}\,cm^{-3}$) above the VBM (Section 4.2). For the N-doped ($N_D=10^{20}\,cm^{-3}$) diamond, our calculations predict the bulk Fermi level at 1.6 eV [51] below the CBM, 0.1 eV above the deep donor level. The band-bending widths have been calculated in Section 4.2 and are listed in Table 1. The shift of the C 1s core levels from Refs. [23,53] and Figs. 7 and 8 allow the change in band bending to be determined. The simulated band-bending values and the values determined earlier by UPS and by the C 1s shifts [37] allow the absolute band bending (as listed in Table 2) to be determined. The UPS results from Figs. 10–13 allow the electron

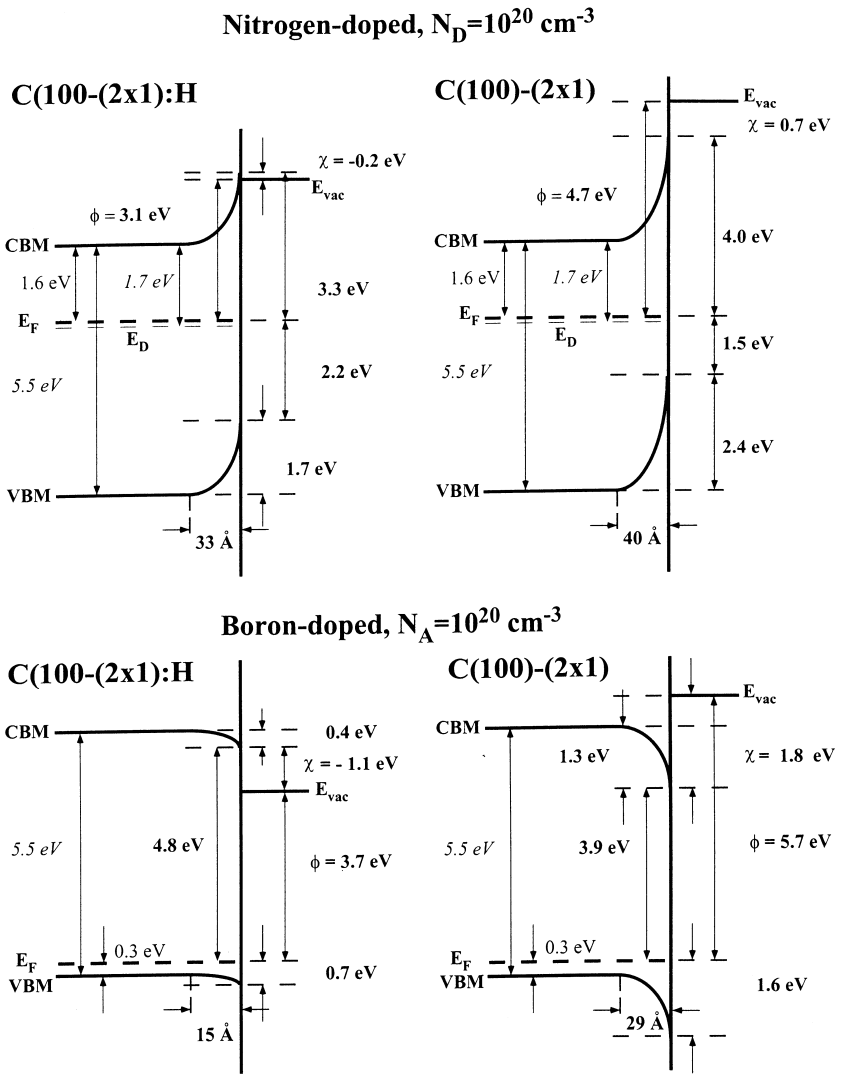

Fig. 18. Band diagrams of the high (a) boron- and (b) nitrogen-doped H-terminated and H-free diamond (100) surfaces. The values are estimated to lie within an error value of 0.1 eV. The values from the literature are shown in italics, the calculated values in normal font and the measured values in bold.

affinity χ and the work function, ϕ, of the differently terminated, doped and oriented diamond surfaces to be determined, as summarized in Table 3.

All the H-terminated diamond surfaces show NEA, whereas the H-free surfaces present PEA. The work function of the B-doped diamond (100) surfaces is slightly larger than for the N-doped surface. Similar results were found for p- and n-type silicon surfaces [46,70,71]. Cardona and Ley [46] note that the work function ϕ of semiconductors is defined with respect to its Fermi level, which can be altered by doping or by surface reconstruction. The different work function values result from the fact that the Fermi level, E_F, at the surface is not pinned exactly in the middle of the band gap. Whereas, for the p-type surface, E_F is nearer to the VBM, E_F of the n-type surface

is nearer to the CBM [46,70,71]. The differently pinned Fermi levels for the hydrogen-terminated N- and B-doped surfaces is due to the fact that hydrogen removes the π-type surface states, inducing a flattening of the bands at the surface. The (100)-(2 × 1):H surfaces have a work function approximately 1.5 eV lower than the (100)-(2 × 1) surfaces. Similarly to alkalis on metal surfaces, hydrogen termination with C–H bonds at the surface results in a strong dipole layer, decreasing ϕ of the diamond (100) surface by approximately 1.5 eV. It is then a logical consequence that we observe a slightly different NEA value for the N- and B-doped diamond (100) surfaces. The quantity that changes similarly for the two different terminated N- and B-doped diamond (100) surfaces is the work function. The energy distance, $E_F - CBM$, and the band bending change differently because of the doping of the crystals and because of the different crystals (natural and synthetic crystals with various doping concentrations have different quantities of defects).

The NEA peak, however, is only detected for the B-doped diamond (100)-(2 × 1):H surfaces, whereas it is not detected for the high-N-doped diamond (100)-(2 × 1):H surface due to a large upward band bending. For the low-B-doped diamond (111)-(1 × 1):H surface, the NEA peak is absent due to the $k_\parallel$-conservation in photoemission. The present results suggest the following view on the mechanism of NEA diamond surfaces. N- and B-doped diamonds with hydrogen-terminated (100) surfaces present NEA due to the wide band gap (5.5 eV) and due to the reduced work function because of hydrogen termination. In addition, the B-doped diamond (100)-(2 × 1):H surface shows a downward band bending, and therefore, the electrons emitted from the CBM can easily escape into the vacuum by forming a high-intensity peak, as observed experimentally by UPS. In contrast to the B-doped (100)-(2 × 1):H surface, UPS measurements on the N-doped (100)-(2 × 1):H surface do not reveal a high-intensity NEA peak due to the strong upward band bending.

5. Conclusions

In summary, we investigated, using photoelectron spectroscopy, the band bending, electron affinity and work function of differently terminated, oriented and doped diamond surfaces. The H-terminated diamond surfaces have NEA, whereas the H-free surfaces present PEA. The high-intensity NEA peak probed by UPS is only observed for the B-doped diamond (100) surfaces, whereas it is not visible for the N-doped diamond (100) surface due to the high upward band bending and for the B-doped diamond (111) surface due to the $k_\parallel$ conservation in photoemission.

Electron emission from energy levels below the CBM up to the vacuum level E_{vac} allowed the electron affinity to be measured quantitatively for PEA as well as for NEA. The emission from populated surface states forms a shoulder or peak at low kinetic energies depending on the NEA and revealing a dispersion behavior. The low-B-doped diamond (100)-(2 × 1):H surface presents a high-intensity NEA peak, with a FWHM of 250 meV, resulting in an upper limit NEA value of −1.0 eV. The high-B-doped diamond (100) surface behaves similarly, showing that NEA is present due to the wide band gap, the downward band bending and the reduced work function because of hydrogen termination. The N-doped (100)-(2 × 1):H surface shows a low NEA of −0.2 eV but no NEA peak due to the strong upward band bending. No NEA peak is measured for the B-doped (111)-(1 × 1):H surface according to the $k_\parallel$ conservation in photoemission, but the surface presents an upper limit NEA value of −0.9 eV. By studying the role of doping concentration, surface orientation and surface adsorbent for the transport and escape of electrons in the emission process, an emission model has been deduced for different diamond surfaces summarized in the energy band diagrams. The emission model suggests that the high-intensity NEA peak of the B-doped diamond (100)-(2 × 1):H surface seems to be due to the downward band bending, together with the reduced work function because of hydrogen termination, taking into account that the condition of $k_\parallel$ conservation in photoemission is satisfied. The work function increases for subsequent hydrogen desorption at higher annealing temperatures with associated loss of NEA. For the N-doped diamond (100) surface, the electron affinity and work function behave similarly, but the observation of an NEA peak is

absent because of the surface barrier formed by the upward band bending.

Acknowledgements

We thank C. Nützenadel for the AFM/STM measurements, J. Ristein, J. Hayoz and Th. Pillo for the fruitful discussions and F. Bourqui, C. Neururer, E. Mooser and O. Raetzo for the skillful technical assistance. The authors gratefully acknowledge financial support by the Swiss Priority Program Materials and the Swiss National Science Foundation. Part of this work was carried out under the auspices of the trinational "D–A–CH" cooperation of Germany, Austria, and Switzerland on the "Synthesis of Superhard Materials".

References

[1] J.E. Field, The Properties of Natural and Synthetic Diamond, Academic Press, London, 1992.
[2] M.A. Prelas, G. Popovici, L.K. Bigelow, Handbook of Industrial Diamonds and Diamond Films, Marcel Dekker, New York, 1998.
[3] L.S. Pan, D.R. Kania, Diamond: Electronic Properties and Applications, Kluwer Academic, Boston, MA, 1995.
[4] G. Davies, Properties and Growth of Diamond, Short Run Press, Exeter, UK, 1994.
[5] S. Koizumi, M. Kamo, Y. Sato, H. Ozaki, T. Inuzuka, Appl. Phys. Lett. 71 (1997) 1065.
[6] R.G. Farrer, Solid State Commun. 7 (1969) 685.
[7] S.A. Kajihara, A. Antonelli, J. Bernholc, Phys. Rev. Lett. 66 (1991) 2010.
[8] K. Okano, S. Koizumi, S. Ravi, P. Silva, G.A.J. Amaratunga, Nature 381 (1996) 140.
[9] W. Geis, J.C. Twichell, N.N. Efremow, K. Krohn, T.M. Lyszczarz, Appl. Phys. Lett. 68 (1996) 2294.
[10] M.W. Geis, J.C. Twichell, J. Macaulay, K. Okano, Appl. Phys. Lett. 67 (1995) 1328.
[11] M.W. Geis, J.C. Twichell, T.M. Lyszczarz, J. Vac. Sci. Technol. B 14 (1996) 2060.
[12] P. Lerner, P.H. Cutler, N.M. Miskovsky, J. Vac. Sci. Technol. B 15 (1997) 337.
[13] C. Bandis, B.B. Pate, Phys. Rev. B 52 (1995) 12056.
[14] R.L. Bell, Negative Electron Affinity Devices, Clarendon, Oxford, 1973.
[15] J.J. Scheer, J. van Laar, Solid State Commun. 3 (1965) 189.
[16] R.U. Martinelli, Appl. Phys. Lett. 16 (1970) 261.
[17] B. Goldstein, Surf. Sci. 35 (1973) 227.
[18] F.J. Himpsel, J.A. Knapp, J.A. VanVechten, D.E. Eastmann, Phys. Rev. B 20 (1979) 624.
[19] B.B. Pate, Surf. Sci 165 (1986) 83.
[20] J. van der Weide, Z. Zhang, P.K. Baumann, M.G. Wensell, J. Bernholc, R.J. Nemanich, Phys. Rev. B 50 (1994) 5803.
[21] C. Bandis, B.B. Pate, Surf. Sci. 350 (1996) 315.
[22] R.E. Thomas, T.P. Humphreys, C. Pettenkofer, D.P. Malta, J.B. Posthill, M.J. Mantini, R.A. Rudder, G.C. Hudson, R.J. Markunas, in: D.L. Dreifuss et al. (Eds.), Diamond for Electronic Applications, MRS Symposia Proc. No. 416, Materials Research Society, Boston, MA, 1996, p. 263.
[23] L. Diederich, O.M. Küttel, E. Maillard-Schaller, L. Schlapbach, Surf. Sci. 349 (1996) 176.
[24] J. van der Weide, R.J. Nemanich, J. Vac. Sci. Technol. B 10 (1992) 1940.
[25] C. Bandis, D. Haggerty, B.B. Pate, in: C.H. Charter, Jr., G. Gildenblat, S. Nakamura, R.J. Nemanich (Eds.), Diamond, SiC and Nitride Wide Bandgap Semiconductors, MRS Symposia Proc. No. 339 Materials Research Society, Pittsburgh, PA, 1994, p. 75.
[26] D.P. Malta et al., in: C.H. Charter, Jr., G. Gildenblat, S. Nakamura, R.J. Nemanich (Eds.), Diamond, SiC and Nitride Wide Bandgap Semiconductors, MRS Symposia Proc. No. 339 Materials Research Society, Pittsburgh, PA, 1994, p. 39.
[27] R.J. Nemanich, P.K. Baumann, M.C. Benjamin, S.W. King, J. van der Weide, R.F. Davis, Diamond Relat. Mater. 5 (1996) 790.
[28] L. Diederich, O.M. Küttel, P. Aebi, E. Maillard-Schaller, R. Fasel, L. Schlapbach, Diamond Relat. Mater. 7 (1998) 660.
[29] W.E. Pickett, Phys. Rev. Lett. 73 (1994) 1664.
[30] Z. Zhang, M. Wensell, J. Bernholc, Phys. Rev. B 51 (1995) 5291.
[31] M.R. Vilar, G. Blatter, P. Pfluger, M. Heyman, M. Schott, Europhys. Lett. 5 (1988) 375.
[32] D.A. Lapiano-Smith, E.A. Eklund, F.J. Himpsel, Appl. Phys. Lett. 59 (1991) 2174.
[33] M.C. Benjamin, C. Wang, R.F. Davis, R.J. Nemanich, Appl. Phys. Lett. 64 (1994) 3288.
[34] M.J. Powers, M.C. Benjamin, L.M. Porter, R.J. Nemanich, R.F. Davis, J.J. Cuomo, G.L. Doll, S.J. Harris, Appl. Phys. Lett. 67 (1995) 3912.
[35] J. Osterwalder, T. Greber, A. Stuck, L. Schlapbach, Phys. Rev. B 44 (1991) 13764.
[36] O.M. Küttel, R.G. Agostino, R. Fasel, J. Osterwalder, L. Schlapbach, Surf. Sci. 312 (1994) 131.
[37] L. Diederich, O.M. Küttel, E. Leroy, Th. Pillo, P. Ruffieux, P. Aebi, L. Schlapbach, Surf. Sci. 417 (1998) 41.
[38] O.M. Küttel, L. Diederich, E. Schaller, O. Carnal, L. Schlapbach, Surf. Sci. 337 (1995) L812.
[39] L. Diederich, O.M. Küttel, P. Aebi, E. Maillard-Schaller, Ch. Nützenadel, R. Fasel, L. Schlapbach, in preparation.
[40] B.D. Thoms, M.S. Owens, J.E. Butler, C. Spiro, Appl. Phys. Lett. 65 (1994) 2957.
[41] C. Nützenadel, O.M. Küttel, L. Diederich, E. Maillard-

Schaller, O. Gröning, L. Schlapbach, Surf. Sci. 369 (1996) L111.
[42] P.G. Lurie, J.M. Wilson, Surf. Sci. 65 (1977) 453.
[43] G. Schober, O. Weis, Surf. Sci. 383 (1997) 203.
[44] K. Hayashi, S. Yamanaka, H. Okushi, K. Kajimura, Diamond Relat. Mater. 5 (1996) 1002.
[45] D. Naumovic, A. Stuck, T. Greber, J. Osterwalder, L. Schlapbach, Phys. Rev. B 47 (1993) 7462.
[46] M. Cardona, L. Ley, Photoemission in Solids I, Springer, Berlin, 1978.
[47] L. Diederich, P. Aebi, O.M. Küttel, E. Maillard-Schaller, R. Fasel, L. Schlapbach, Surf. Sci. 393 (1997) L77.
[48] E.C. Lightlowlers, A.T. Collins, J. Phys. D 9 (1976) 951.
[49] A.T. Collins, A.W.S. Williams, J. Phys. C 4 (1971) 1789.
[50] C. Bandis, Ph.D. thesis, Washington State University, 1994.
[51] L. Diederich, J. Ristein, O.M. Küttel, L. Ley, L. Schlapbach, in preparation.
[52] S.M. Sze, Physics of Semiconductor Devices, 2nd ed., Wiley, New York, 1981.
[53] R. Graupner, J. Ristein, L. Ley, Surf. Sci. 320 (1994) 201.
[54] B.B. Pate, M. Oshima, J.A. Slberman, G. Rossi, I. Lindau, W.E. Spicer, J. Vac. Sci. Technol. A 2 (1984) 957.
[55] J.F. Morar, F.J. Himpsel, G. Hollinger, J.L. Jordan, G. Hughes, F.R. McFeely, Phys. Rev. B 33 (1986) 1340.
[56] R.G. Cavell, S.P. Kowalczyk, L. Ley, R.A. Pollak, B. Mills, D.A. Shirley, W. Perry, Phys. Rev. 7 (1973) 5313.
[57] F.R. McFeely, S.P. Kowalczyk, L. Ley, R.G. Cavell, R.A. Pollak, D.A. Shirley, Phys. Rev. 9 (1974) 5268.
[58] A. Mansour, G. Indlekofer, P. Oelhafen, Appl. Surf. Sci. 48–49 (1991) 312.
[59] W.E. Spicer, Phys. Rev. 112 (1958) 114.
[60] P.J. Dean, E.C. Lightlowlers, D.R. Wright, Phys. Rev. 140 (1965) 352.
[61] G.W. Gobeli, F.G. Allen, E.O. Kane, Phys. Rev. 12 (1964) 94.
[62] E.O. Kane, Phys. Rev. 12 (1964) 97.
[63] C. Bandis, B.B. Pate, Phys. Rev. Lett. 74 (1995) 777.
[64] J. Yater, A. Shih, R. Abrams, Phys. Rev. B 56 (1997) R4410.
[65] J. Furthmüller, J. Hafner, G. Kresse, Phys. Rev. B 53 (1996) 7334.
[66] B.N. Davidson, W.E. Pickett, Phys. Rev. B 49 (1994) 11253.
[67] D.R. Alfonso, D.A. Drabold, S.E. Ulloa, Phys. Rev. B 51 (1995) 14669.
[68] G.D. Kubiak, K.W. Kolasinski, Phys. Rev. B 39 (1989) 1381.
[69] J.F. Morar, F.J. Himpsel, G. Hollinger, J.L. Jordan, G. Hughes, F.R. McFeely, Phys. Rev. B 33 (1986) 1346.
[70] L.F. Wagner, W.E. Spicer, Phys. Rev. B 9 (1974) 1512.
[71] L. Ley, J. Ristein, J. Schäfer, S. Miyazaki, J. Vac. Sci. Technol. B 14 (1996) 3008.